Development of a Mechanical Semi-Active Vibration Absorber

Zhenbang Xu, Xinglong Gong* and Xianmin Chen

CAS Key Laboratory of Mechanical Behavior and Design of Materials, Department of Modern Mechanics, University of Science and Technology of China, Hefei 230027, China

xuzhb@mail.ustc.edu.cn; gongxl@ustc.edu.cn

Abstract

A Semi-Active Vibration Absorber (SAVA) can suppress the vibration with time-varying frequency by tuning its natural frequency to track the excitation frequency. This paper presents the development of a mechanical SAVA whose natural frequency can be adjusted in real time by adjusting its geometry parameters. The principle and dynamic properties of the SAVA were theoretically analyzed. Based on these analyses, a prototype SAVA was designed and implemented. An optimum variable step-size control strategy of the SAVA was investigated. This control strategy is made up by two stages: the roughly tuning stage and the optimization stage. Some experiments were conducted to evaluate the dynamic properties and vibration attenuation performance of the SAVA. The experimental results indicate that the developed SAVA can tune its natural frequency in a large frequency range and its vibration attenuation effect is significantly improved compared with a Tuned Vibration Absorber (TVA).

Keywords: Semi-active vibration absorber, Optimum variable step-size control strategy, Vibration attenuation effect

1 Introduction

Tuned Vibration Absorbers (TVAs) are widely used in industries to suppress undesirable vibrations of some machines excited by harmonic forces. However, these TVAs are only effective over a narrow frequency range. As the excitation frequency varies, the vibration attenuation effect of the TVA decreases or even collapses because of mistune. This problem limits many applications of the TVAs. One of solutions to this problem is to develop a Semi-Active Vibration Absorber (SAVA). The SAVA can improve the vibration attenuation performance significantly by adjusting its natural frequency in real time to track the excitation frequency. Without an active force, the SAVA consumes less power than the active vibration absorber. Moreover, the SAVA is a fail-safe device as it can work as a TVA in case of loss of power.

Currently, a variety of ways have been used in semi-active vibration control, such as variable stiffness element through mechanical mechanisms[1–4], variable magnetic element controlled by current[5,6] or using controllable new materials[7–11]. The variable stiffness elements through mechanical mechanisms have some advantages of good stability, long-life running and easily available material, therefore it is more suitable as the stiffness element of the SAVA. A SAVA[1] was developed which used helical spring as the tunable stiffness element. The stiffness of the element can be adjusted by changing the effective number of coils. The stiffness of a cantilever beam depends on its effective length, therefore it can serve

*Corresponding author.

as a tunable stiffness element of SAVA[2]. Adjusting the effective length of the beam with a motor can tune the natural frequency of the SAVA. Two leaf-springs were used to construct a tunable stiffness element[3] whose stiffness can be adjusted by controlling the opening of two leaf-springs. Bonello *et al.*[4] proposed a SAVA with piezo-actuated curved beam whose stiffness is varied by adjusting the curvature of the beam. Such a SAVA has the advantages of having small redundant mass and tracking excitation frequency rapidly. However, it consumes more energy to achieve the variable stiffness compared with other mechanical SAVA.

The control strategies of natural frequency of the SAVA have been the subjects of some researches. A robust tuning strategy[1] was presented for adaptive control. It was based on minimizing the voltage amplitude from an accelerometer. To identify the excitation frequency accurately, a control method was developed[12] by making use of informations of both the response spectrum and the natural frequencies of the primary system. Kidner *et al.*[13] designed a nonlinear fuzzy logic controller for the SAVA using the phase difference between the velocities of the absorber mass and the host structure.

In this study, a mechanical SAVA was developed. It meets the practical application specifications: low structural damping, small size and small redundant mass. An optimum variable step-size control strategy was studied for improving the control performance. To evaluate the tuning characteristic and the vibration attenuation effect of the SAVA, some experiments were carried out.

2 Working Principle and Mechanical Structure

2.1 Working principle

2.1.1 Principle of frequency-shift

Figure 1 is a schematic diagram of the SAVA which is composed of two spring poles and an absorber mass. The spring poles can deform along the axial direction when compressed or prolonged. The element subjected to the load F_0 deforms as shown in Fig. 1. Δy is the displacement of the absorber mass in force direction.

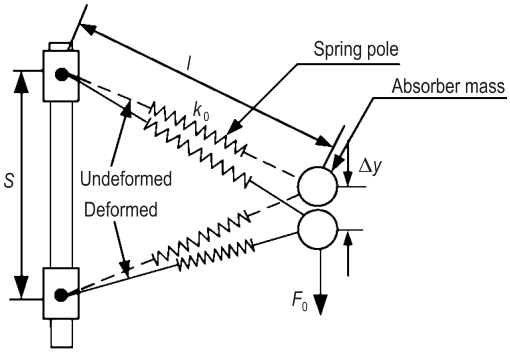

Fig. 1 Schematic diagram of the SAVA

In order to obtain the relationship between the equivalent stiffness of the SAVA and the span between two spring poles, an approximate analysis is implemented based on the small deformation hypothesis. If the deformation is sufficiently small, the equivalent stiffness of the element k_e is given by:

$$k_e = \frac{F_0}{\Delta y} = \left(\frac{S}{l}\right)^2 \frac{k_0}{2} \tag{1}$$

where l is the length of the spring pole, S is the span and k_0 is the stiffness of the spring pole. The natural frequency of the SAVA can be obtained as:

$$f_e = \frac{1}{2\pi}\sqrt{\frac{k_e}{m}} = \frac{S}{2\pi l}\sqrt{\frac{k_0}{2m}} \tag{2}$$

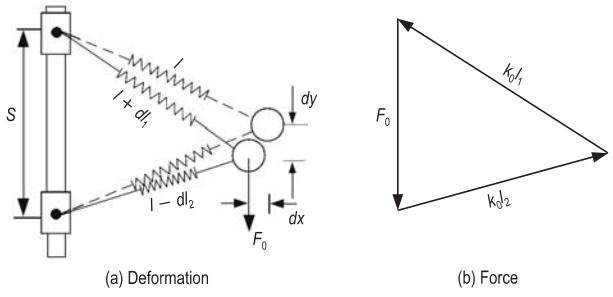

Fig. 2 Deformation and force analysis of the SAVA

where m is the mass of the absorber mass. From (2), the natural frequency varies as the span linearly. The larger the span is, the higher the frequency, and vice versa. Therefore, the natural frequency of the SAVA can be tuned by adjusting the span in real time.

2.1.2 Non-linearity

With the vector operational method and simple geometrical relationship, the exact relationship between the force and the deformation can be achieved. Figure 2 shows the deformation and force analysis of the SAVA. As shown in this figure, when the force F_0 is applied to the absorber mass, the spring poles deform and finally reach a balanced state. The proportional relation of the force and the deformation can be expressed as:

$$\frac{k_0 dl_1}{l + dl_1} = \frac{k_0 dl_2}{l - dl_2}; \quad \frac{F_0}{S} = \frac{k_0 dl_2}{l - dl_2} \tag{3}$$

Then the deformation of the poles can be derived as:

$$dl_1 = \frac{F_0 l}{k_0 S - F_0}, \quad dl_2 = \frac{F_0 l}{k_0 S + F_0} \tag{4}$$

Defining the original position is the end at no force applied, then the end displacements at the force F_0 is given by:

$$\begin{cases} dx = \frac{\sqrt{4l^2 - S^2}}{2} - \sqrt{1 - \frac{\left(\left(l - \frac{F_0 l}{k_0 S + F_0}\right)^2 + S^2 - \left(l - \frac{F_0 l}{k_0 S - F_0}\right)^2\right)^2}{4\left(l - \frac{F_0 l}{k_0 S + F_0}\right)^2 s^2}} \left(l - \frac{F_0 l}{k_0 S + F_0}\right) \\ dy = \frac{2S^2 l^2 k_0^3 F_0}{(k_0 S + F_0)^2 (k_0 S - F_0)^2} \end{cases} \tag{5}$$

As stated previously, there is a linear relation between the force F_0 and approximate deformation Δy. Therefore, the linearity between the force F_0 and accurate deformation dy can be analyzed by using the ratio of exact and approximate deformation $dy/\Delta y$.

Fixing the ratios of span and pole length S/l are 0.2, 0.4, 0.8 and 1.6, the ratios of exact and approximate deformation $dy/\Delta y$ at different deformations dy/l are given in Fig. 3. As can be seen from this figure, when the ratio of span and spring pole length is small, the system has good linearity even though the

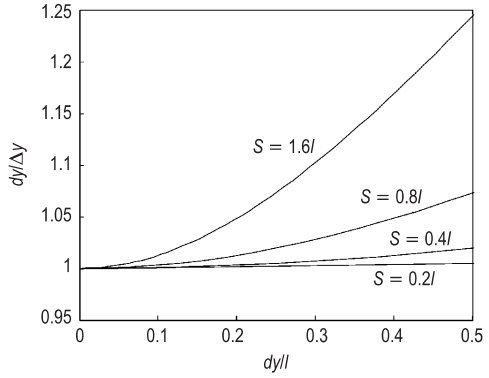

Fig. 3 The ratios of exact and approximate deformation with different spans

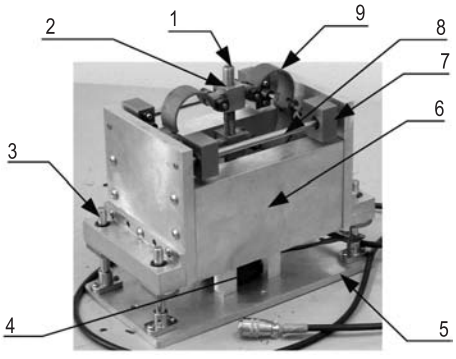

Fig. 4 The photograph of the SAVA. 1. Screw rod 2. Screw cap 3. Vertical guide 4. Step motor 5. Base 6. Absorber mass 7. Horizontal slider 8. Horizontal guide 9. Leaf spring

displacement of absorber mass reaches the half of the pole length. Conversely, when the span is as large as the spring pole length, the system linearity becomes poor as the displacement increases. If the displacement of absorber mass is less than 10% of the pole length ($dy/l \leq 10\%$), the error between exact and approximate deformation is less than 1% even though the ratio of span and pole length is $1.6(S = 1.6l)$. From the above analysis, if the span is less than the pole length and the displacement of absorber mass is less than 10% of pole length, the system has good linearity.

2.2 Mechanical structure of the prototype

Figure 4 is a photograph of the SAVA prototype. The absorber mass of the prototype is a closed configuration which is composed of four individual masses. There are two horizontal guides mounted on the absorber mass. Four horizontal sliders can move in horizontal direction along the two horizontal guides. This configuration can make the best use of the space and reduce the size of the SAVA. The masses are made of duralumin alloy.

The leaf spring is chosen as the spring pole because of the large bear load and lateral rigidity. The stiffness element of the SAVA is composed of four leaf springs. One edge of the spring is linked to the screw cap with a pin, and the other is linked to the horizontal slider with a pin. When the step motor drives the screw rod to rotate, two screw caps move toward or away from each other along the screw rod. Thus, the span between leaf springs can be changed, which causes the natural frequency of the SAVA changed.

Four vertical guides, mounted on the base, are used to make the absorber mass to move only in vibration direction. The mass of the absorber mass is about 4 kilograms, and the other mass is about 1 kilogram. The mass utilization ratio of the SAVA is about 80%.

3 Control Strategy of the SAVA

An adaptive control strategy of SAVA is to tune the natural frequency of the SAVA to the same value as the excitation frequency. However, both experimental errors and the property changes of SAVA caused by

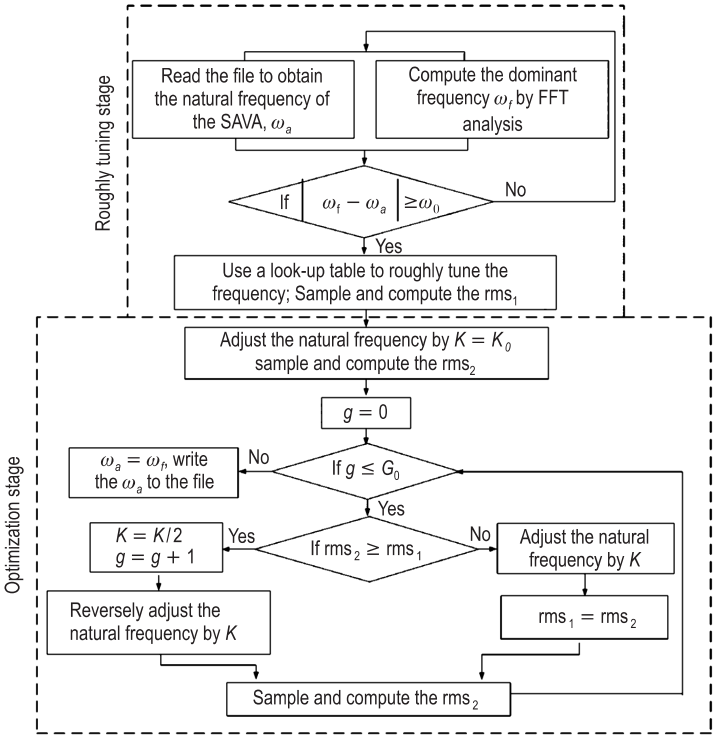

Fig. 5 Flow chart of the control strategy

long time running make it difficult to adjust natural frequency to coincide with the excitation frequency accurately. To address the issue, an optimum variable step-size control strategy was developed in the present study. The strategy includes two stages: the roughly tuning stage and the optimization stage. The object of the roughly tuning is to guarantee the control speediness; and the object of the optimization is to improve the control accuracy. Figure 5 is the flow chart of the control strategy.

Prior to the start of the control process, the initial frequency of the SAVA, the relational table between the natural frequency and the span and the initial optimization step size must be set. In the roughly tuning stage, the control system obtains the dominant frequency by FFT, then uses a look-up table to compute the desired span, and drives the motor to tune the span. By this way, the control system can adjust the frequency of the SAVA to the vicinity of the exciting frequency as quickly as possible.

After the roughly tuning stage, the control system implements the optimum variable step-size control. The object of the control is to minimize the Root Mean Square (RMS) of the primary system's vibration. The rms can be expressed as:

$$rms = \sqrt{\frac{\sum_{i=1}^{N} a_i^2}{N}} \tag{6}$$

where a_i is the sampled acceleration response and N is the total number of samples in the time interval of interest. In the optimization stage, sampling and computing the rms must be carried out after every

adjustment. If the new rms is greater than the previous least one, which means the adjustment direction is wrong, the direction of next adjustment will be changed, the step size will be halved and the counter will be increased by 1. Otherwise, the next adjustment keeps the same direction and step size, and the least rms will be updated. The control process stops when g is greater than G_0. g is a counter number. G_0 is a flag which indicates the end of the control. It also decides the control accuracy. The larger the value of G_0, the higher the control accuracy.

In Fig. 5, ω_0 is a threshold. When the difference between the natural frequency of the SAVA and the excitation frequency is bigger than ω_0, the control system considers the tuning condition are not met and start to tune the SAVA. K and K_0 are optimization step size and initial optimization step size, respectively. $rms_1(rms_2)$ denotes root mean square of the primary system's vibration.

4 Experimental Evaluations

4.1 Experimental evaluation of frequency-shift property

The set-up for evaluating the frequency-shift property of the frequency-shift property of the SAVA is shown in Fig. 6. The SAVA was fixed on a vibration table. The signal analyzer (model: Signal Calc ACE DP240, Data Physics Corp.) provided an excitation signal to drive the system via a power amplifier. Two accelerometers (model: CA-YD, manufactured by Sinocera Piezotronics Inc., china) were placed on the absorber mass and the vibration table to measure their responses, respectively.

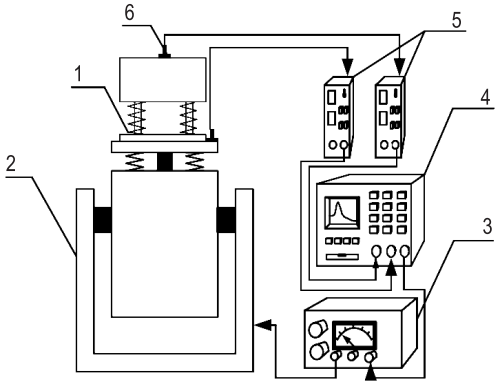

Fig. 6 The set-up for evaluating the frequency-shift property. 1. SAVA 2. Vibration table 3. Power amplifier of the vibration table 4. Signal analyzer 5. Charge amplifier 6. Acceleration transducer

The acceleration signal of the absorber mass was sent to the signal analyzer as the output signal of the SAVA, and that of the vibration table was sent to the signal analyzer as the input signals of the SAVA. With the input and output signals, the transmissibility, relating the acceleration of the absorber mass to the acceleration of the vibration table, can be obtained by using FFT analysis. The peak position of the transmissibility curve is the natural frequency of the SAVA.

For each span setting, swept-frequency signal excitation was applied and the transmissibility was measured. Figure 7(a) shows the amplitude-frequency curve of the transmissibility, and Fig. 7(b) shows the phase-frequency curve of the transmissibility. It can be seen that the transmissibility curves all move rightward with the increase in the span, which means the natural frequency of the SAVA varies as the span. By reading the peak value of the transmissibility in Fig. 7(a), the frequency-shift property of the SAVA is obtained shown in Fig. 8. As shown in this figure, the natural frequency of the SAVA increases remarkably when the span increases. The natural frequency changes from 20.25 Hz to 36.5 Hz when the span changes from 26 mm to 62 mm, thus, the SAVA has a capability to change its frequency by 180%. Moreover, the frequency-shift property has well linearity.

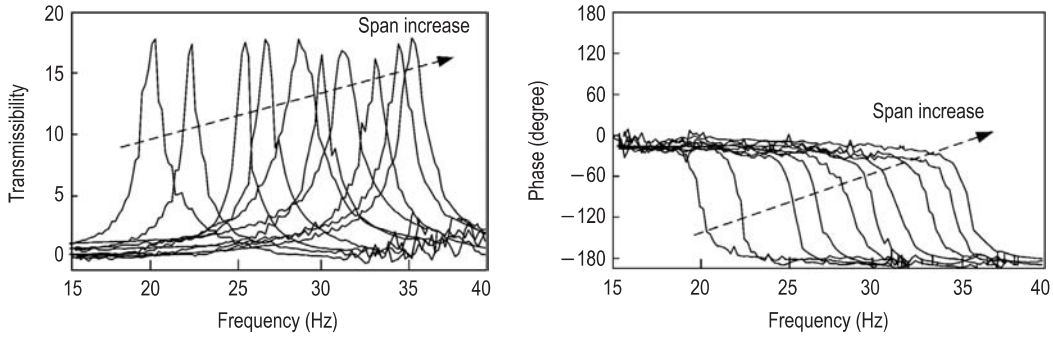

(a) Amplitude-frequency curve of the transmissibility (b) Phase-frequency curve of the transmissibility

Fig. 7 The transmissibility versus frequency at various spans

4.2 Experimental evaluation of the vibration attenuation performance of the SAVA

Figure 9 shows the schematic of the experimental set-up for evaluation of the vibration attenuation performance of the SAVA. A clamped-clamped beam with a pullback weight attached was used as the primary system. The first mode of the beam is bending vibration and the natural frequency of mode is about 35 Hz. The SAVA was mainly used to control this mode vibration, so it was placed at the center of beam where the vibration is the largest.

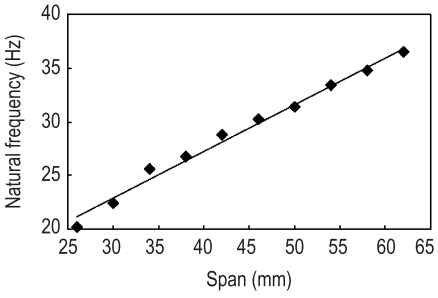

Fig. 8 The frequency-shift property of the SAVA. ♦ experimental data; —fitting curve

As shown in Fig. 9, an impedance head connects with the beam and the exciter, and it measures the force signal and the acceleration signal which is used as the input of the controller. The ratio of the force signal and the acceleration signal is the acceleration admittance of the beam. With an absorber attached, the dynamic property of the beam changes and hence the admittance of the beam changes. Therefore, the vibration attenuation effect of an absorber can be represented by comparing the admittance of the beam with and without absorber. The effect is expressed as:

$$\gamma = 20\lg(|H_A/H_o|) \tag{7}$$

where H_A, H_o are the admittances with and without absorber, respectively. In the experiment, the system was excited with a series of single frequencies to approximate a swept harmonic excitation. The frequency range of the excitation is 20 Hz–40 Hz.

The system in Fig. 9 can be simplified as shown in Fig. 10. M_B is the mass of beam and M_A is the absorber mass. Lumped mass M_s is the summation of the pullback weight mass and the redundancy mass of the absorber. K^* is the complex stiffness of the absorber. The beam and lumped mass are looked as vibration controlled object. With the similar methods in literature[14], the admittances with and without absorber can be achieved.

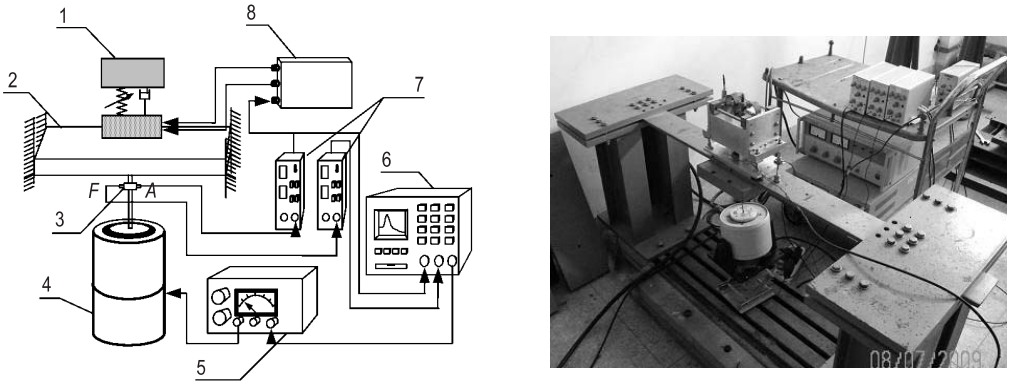

(a) Scheme (b) Photograph

Fig. 9 Experimental set-up for evaluating the vibration attenuation performance of the SAVA. 1. SAVA 2. Clamped-clamped beam 3. Impedance head 4. Exciter 5. Power amplifier of the exciter 6. Signal analyzer 7. Charge amplifier 8. Control system of the SAVA

Without the absorber and lumped mass, the admittance of the beam at the point O is:

$$H_o^b = \frac{V_o^b}{F_o^b} = \frac{j\omega}{M_B} \sum_{k=1}^{n} \frac{\Phi_k^2(x_o)}{\omega_k^2(1+j\eta) - \omega^2} \tag{8}$$

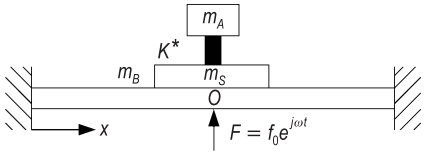

Fig. 10 Simplified model of the evaluation system

where F_o^b and V_o^b are the amplitude of excitation force and the velocity at point O, respectively, ω_k, Φ_k are the kth natural frequency and mode function of the beam, respectively, x_o is the coordinate position of the point O, n is the number of the mode which is taken into account, η is the loss factor of beam, ω is the angular frequency of excitation force.

With the absorber mass and the lumped mass, F_o is the excitation force, V_o is the velocity of the beam, F_s^b and V_s^b are the force and the velocity on the base of the lumped mass, F_s^t and V_s^t are those on the top of the lumped mass. F_A and V_A are force and the velocity on the absorber mass, then

$$V_o = H_o^b(F_o - F_s^b) \tag{9}$$

The force and velocity equations of lumped mass are:

$$V_s^b = V_s^t = V_o, \quad F_s^b + F_s^t = j\omega M_s V_s^t \tag{10}$$

The dynamic equations of the absorber are:

$$F_A = -F_s^t, F_A = -\frac{K^*}{j\omega}(V_A - V_s^t), \quad F_A = j\omega M_A V_A \tag{11}$$

According to (9), (10) and (11), the following can be obtained:

$$V_o = \frac{\Delta H}{H_o^b + \Delta H} H_o^b F_o, \quad \Delta H = 1/\left(j\omega M_s + \frac{j\omega M_A K^*}{K^* - \omega^2 M_A}\right) \tag{12}$$

where ΔH is the additional admittance at point O due to the absorber and lumped mass. The admittance at point O is:

$$H_A = \frac{\Delta H}{H_o^b + \Delta H} H_o^b \tag{13}$$

For metallic structure, the structural damping is more accurate than viscous damping, so the spring of the absorber is looked as an element with complex stiffness. The complex stiffness K^* can be expressed by conventional spring's stiffness K and damping ratio ξ:

$$K^* = K(1 + 2\xi j) \tag{14}$$

For the TVA, the stiffness of the absorber K is a constant and $K = \omega_1^2 m_a$, ω_1 is the first natural frequency of the beam. For the SAVA, the stiffness of the absorber varies with the excitation frequency and $K = \omega^2 m_a$.

According to (12), (13), the admittance on point O without the absorber is:

$$H_o = \frac{\Delta H^s}{H_o^b + \Delta H^s} H_o^b, \quad \Delta H^s = 1/(j\omega M_s) \tag{15}$$

By comparing the admittances on point O with and without absorber, the vibration attenuation effect can be evaluated by (7).

For harmonic vibration, the ratio of the velocity admittances is equal to the ratio of the acceleration admittances. The comparison of vibration attenuation effect between the SAVA and TVA is shown in Fig. 11, where the upper data are the results of the TVA whose natural frequency is fixed to the first natural frequency of the beam and the lower data are the results of the SAVA whose natural frequency is tuned to trace the excitation frequency. As shown in Fig. 11, for the TVA, the best vibration attenuation effect occurs at the natural frequency of the beam. When the excitation frequency is apart from this frequency, the effect becomes bad sharply and the vibration near to the 26 Hz is even larger than that without the TVA attached. For the SAVA, the vibration attenuation effect is equal to that of the TVA at the first natural frequency of the beam, and it has better effect in the whole adjustable frequency band. The experimental data and numerical curve are close. It indicates that the dynamic model is reasonable and the experimental data is reliable.

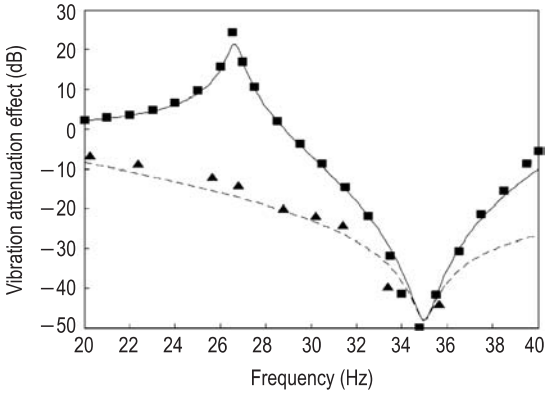

Fig. 11 The vibration attenuation of absorbers. ▲SAVA (experimental data); - - - - - - - -SAVA (numerical data); ■ TVA (experimental data); ——TVA (numerical data)

5 Conclusions

In this paper, a mechanical SAVA was developed. Its natural frequency was tuned by adjusting the span between the ends of two spring poles which support the absorber mass. An optimum variable step-size control strategy was studied which can guarantee the control speediness and improve the control

accuracy. The experimental results of the frequency shift property indicated that the natural frequency of the developed SAVA is linear to the span. When the span changes from 26 mm to 62 mm, the natural frequency of the SAVA can change from 20.25 Hz to 36.5 Hz. To evaluate the vibration attenuation performance of the SAVA, a beam with two ends supported was used as a primary system and the ratio of the admittances of the beam with and without absorber was used as the indicator. The experimental results agreed well with the theoretical calculation and they all demonstrated that the developed SAVA has better vibration attenuation performance than TVA.

References

[1] Franchek, M. A., Ryan, M. W. and Bernhard, R. J., Adaptive passive vibration control, *J. Sound Vibration*, Vol. 189, pp. 565–585, 1995.

[2] Nagaya, K., Kurusu, A., Ikal, S. and Shitani, Y., Vibration control of a structure by using a tunable absorber and an optimal vibration absorber under auto tuning control, *J. Sound Vibration*, Vol. 228, pp. 773–792, 1999.

[3] Walsh, P. L. and Lamancusa, J. S., A variable stiffness vibration absorber for minimization of transient vibrations, *J. Sound Vibration*, Vol. 158, pp. 195–211, 1992.

[4] Bonello, P., Brennan, M. J. and Elliott, S. J., Vibration control using an adaptive tuned vibration absorber with a variable curvature stiffness element, *Smart Materials and Structures*, Vol. 14, pp. 1055–1065, 2005.

[5] Liu, J. and Liu, K., A tunable electromagnetic vibration absorber: Characterization and application, *Journal of Vibration and Acoustics*, Vol. 295, pp. 708–724, 2006.

[6] Gowrisankar, A., Nandi, A., Neogy, S. and Das, A. S., Vibration control of a beam using an eddy current damper with on-off control, *Advances in Vibration Engineering*, Vol. 7, pp. 343–351, 2008.

[7] Rustighi, E., Brennan, M. J. and Mace, B. R., A shape memory alloy adaptive tuned vibration absorber: Design and implementation, *Smart Materials and Structures*, Vol. 14, pp. 19–28, 2005.

[8] Gupta, K., Darpe, A. K., Kumar, B., Bhatia, A., Ahmed, S. M., Aravindhan, T. S. and Nakra, B. C., Resonance control of rotor using shape memory alloys, *Advances in Vibration Engineering*, Vol. 8, pp. 247–254, 2009.

[9] Lerner, A. A. and Cunefare, K. A., Performance of MRE-based vibration absorbers, *Journal of Intelligent Material Systems and Structures*, Vol. 19, pp. 551–563, 2008.

[10] Deng, H. X., Gong, X. L. and Wang, L. H., Development of an adaptive tuned vibration absorber with magnetorheological elastomer, *Smart Materials and Structures*, Vol. 15, pp. N111–N116, 2006.

[11] Seto, K. and Tanaka, T., Seismic response control for multiple buildings connected with MR damper, *Advances in Vibration Engineering*, Vol. 7, pp. 41–49, 2008.

[12] Liu, K., Liao, L. and Liu, J., Comparison of two auto-tuning methods for a variable stiffness vibration absorber, *The Transactions of Canadian Society for Mechanical Engineering*, Vol. 29, pp. 81–96, 2005.

[13] Kidner, M. R. F. and Brennan, M. J., Varying the stiffness of a beam-like neutralizer under fuzzy logic control, *ASME Journal of Vibration and Acoustics*, Vol. 124, pp. 90–99, 2002.

[14] Niu, J. C., Song, K. J. and Lim, C. W., On active vibration isolation of floating raft system, *J. Sound Vibration*, Vol. 285, pp. 391–406, 2005.